

Line-field confocal optical coherence tomography coupled to Artificial Intelligence to identify quantitative biomarkers of facial skin ageing: An exploratory study

Bonnier, Franck¹; Pedrazzani, Mélanie²; Fischman, Sébastien²; Viel, Théo²; Lavoix, Agnes³; Pegoud, Didier³; Nili, Meryem³; Jimenez, Yolande³; Pittet, Jean-Christophe⁴; Ralambondrainy, Samuel¹; Korichi, Rodolphe¹

¹ LVMH Recherche, Saint Jean de Braye, France ; ² DAMAE Medical, Paris, France ; ³ DERMATECH, Tassin-la-Demi-Lune, France ; ⁴ ORION-CONCEPT, Tours, France.

* Bonnier Franck, 185 avenue de Verdun, 45804 Saint Jean de Braye, France, +33 2 38 60 31 32, fbonnier@research.lvmh-pc.com

Abstract

Background: The study aimed at identifying quantitative biomarkers (i.e. histological and cellular parameters) of facial skin ageing by means of *in vivo* Line-field Confocal Optical Coherence Tomography (LC-OCT) 3D imaging coupled to Artificial Intelligence (AI).

Methods: Hundred Caucasian female volunteers evenly distributed in 5 age groups [20,30], [31,40], [41,50], [51,60] and [61,70] years old were included. LC-OCT acquisitions were performed on 3 zones: Cheekbone, temple and mandible. Skin layers thickness and cell morphology (cell density, nuclei volume, nuclei shape and cell network atypia) were derived from 3D stacks using AI based algorithms. Cellular metrics distribution across the viable epidermis were also extracted to witness age-related variations in keratinocytes maturation.

Results: For the mandible, cell surface density (ANOVA $p < 0.001$), nucleus compactness (KRUSKAL WALLIS $p = 0.029$), nucleus volume (KRUSKAL WALLIS $p = 0.011$), standard deviation of nucleus volume (KRUSKAL WALLIS $p < 0.001$) and cell network atypia (ANOVA $p < 0.001$) displayed significant differences between age groups. Similar observations were made for the temple and cheekbone. The spatial distribution of cellular metrics as function of depth highlighted the potential of LC-OCT to quantify abnormalities in keratinocytes maturation in the viable epidermis.

Conclusion: 3D LC-OCT *in vivo* imaging coupled to AI algorithms enabled to quantify several histological and cellular epidermal parameters (metrics) to highlight age-related modifications. The technique resolution provides information about the thickness of layers, however modifications in nuclei volume, compactness and atypia of the cell network have been identified as potential key biomarkers to quantify skin ageing in healthy female volunteers.

Keywords: Healthy skin, ageing; Line-field Confocal Optical Coherence Tomography; non-invasive 3D imaging; 3D quantification; Artificial Intelligence

Introduction.

Ageing is a natural and complex biological process that inevitably affects all organs and structures of the human body. Skin appearance, that defines the perceived age of an individual by others, is the result of multiple modifications at molecular and cellular levels. Visible signs of ageing, notably skin sagging, wrinkles, sunspots, and uneven skin colour can result in a psychological angst from individuals alongside with the change in their body image [1]. Face skin appearance greatly impacts societal interactions, therefore, delaying the appearance of visible signs revealing the stages of ageing has become a major concern in society to improve self-acceptance and prevent societal exclusion. Longevity and anti-ageing are fields of research constantly expanding that are aiming at a better understanding of biological processes. Although, atlases can be used for scoring the severity of these clinical signs (i.e wrinkles and sagging) [2], skin ageing results from the accumulation of molecular damage over time, potentially exacerbated by a combination of intrinsic (genetics, cellular metabolism, hormonal and metabolic processes) and extrinsic factors (chronic light exposure, pollution, ionizing radiation, chemicals, toxins), that makes the correlation between physiological mechanisms involved and visible effects of ageing difficult. Genetic, epigenetic, and lifestyle predispositions have been well studied to provide an overview of causes that can lead to the onset of first clinical signs of ageing. However, it is established that constant exposure to natural and anthropogenic “chemical” environment significantly affects skin physiology and health. Therefore, the exposome factors are increasingly studied as potentiators for skin aging to better understand the role of well-known factors such as sun, pollution, and tobacco to trigger molecular processes that damage the skin structure, leading to the aged skin appearance, but also to identify other factors, less well studied. Actions of reactive oxygen species (ROS), mtDNA mutations, and telomere shortening, as well as hormonal changes are few of parameters studied using advanced omics approaches (genomics, methylomics, metabolomics, proteomics...) to decipher the discrepancies between the biological age (ageing clocks) and the chronological age (civil age).

The reduction in epidermal thickness, flattening of the dermo-epidermal junction and alteration of the dermal structures are the main histological characteristic of skin ageing. While age-related changes in the mechanical properties have been extensively investigated *in vivo* using torsion or suction devices [3], enabling non-invasive, *in vivo*, visualisation of underlying microstructures of the epidermis and dermis remains a challenge to fully comprehend, monitor and quantify the modifications occurring below the surface. High-frequency ultrasound (HFUS) is a well-established cost-effective tool for rapid imaging of skin. Although instruments operating at frequencies 50-75 MHz are popularised nowadays, the resolutions (lateral and axial) achieved are rather suited to investigate the dermis and subepidermal low-echogenic band (SLEB) properties [4]. Other microscopic techniques, i.e. Reflectance Confocal Microscopy (RCM) [5,6], Confocal Laser Scanning Microscopy (CLSM) [7,8] or multiphoton laser scanning microscopy [9] can be used to reach higher definition of skin features in the epidermis and (upper) dermis. Despite, optical techniques provide high resolution of $\sim 1 \mu\text{m}$, depending on the laser source and focusing optics used, the penetration depth can be limited ($\sim 250 \mu\text{m}$) [10]. Optical Coherence Tomography (OCT) is widespread in the biomedical field with a penetration depth of $\sim 2 \text{ mm}$, depending on tissue types. Although, OCT has a substantial advantage compared to other clinical imaging methods such as ultrasound and MRI, its resolution $\sim 7.5 \mu\text{m}$ [11], greatly limits applications for superficial skin analysis, notably to discern single cells and to distinguish the different layers of the epidermis in detail [12]. High-definition OCT (HD-OCT) however enabled to improve isotropic resolution to $\sim 3 \mu\text{m}$ with a penetration depth of $\sim 500 \mu\text{m}$ [13]. In recent years, Line-Field Confocal OCT (LC-OCT) has emerged as a promising device for *in vivo* non-invasive imaging combining the advantages of OCT and optical microscopy, hence a penetration up to a depth of $\sim 500 \mu\text{m}$ and an isotropic resolution of $\sim 1 \mu\text{m}$ are achieved [14]. LC-OCT coupled to Artificial Intelligence (AI) has been reported to investigate age-related modifications in skin [15] while segmentation algorithms are promising methods to derive 3D quantitative parameters such as skin layer thicknesses (SC and epidermis) and keratinocyte network information (nuclei size, shape and density) as well as the thickness and density of the superficial dermis [16].

The objective of this study was to determine specific histological and cellular metrics (parameters) for the non-invasive assessment of facial skin ageing from a large cohort of

Caucasian female volunteers (n=100) to study the potential of LC-OCT to identify quantitative biomarkers for *in vivo* clinical studies.

Materials and Methods.

Study population

Hundred Caucasian female volunteers evenly distributed in 5 age groups [20,30], [31,40], [41,50], [51,60] and [61,70] years old were included in this exploratory study that has been conducted over a 12-week period from May 2021 with a 1-day participation for each volunteer (DERMATECH, France). Among inclusion criteria, a good health condition and subject with I, II or III skin phototype (according to Fitzpatrick's scale) were considered. The study was supervised by the French ethical committee “Comité de protection des personnes sud méditerranée I” according to the principles expressed in the Declaration of Helsinki, and written informed consent was obtained from all participants. DeepLiveTM analysis, i.e. acquisitions using Line-field Confocal Optical Coherence Tomography (LC-OCT®), were done on the cheek bone, temple and inferior jawline (mandible). A randomisation method was used to define the side of the face (left or right) assessed for each subject.

LC-OCT® imaging

Images were collected using a DeepLiveTM system (DAMAE MEDICAL, France) that provides *in vivo* 3D visualisation ([Figure 1](#)). The two-beam Linnik interference microscope equipped with a supercontinuum laser with line illumination at central 800 nm wavelength enables acquisition of tomographic images perpendicular and parallel to the surface of the skin at 8 frames per second with micrometric lateral and axial resolutions [15]. Paraffin oil was used as an immersion medium that matches the refractive index of the skin ($n \sim 1.4$). Pigmented spots were excluded from acquisitions. For the purpose of the study 4 LC-OCT 3D images ($1200 \mu\text{m} \times 500 \mu\text{m} \times 350 \mu\text{m}$) were acquired as stacks of slices parallel to the skin surface with a $1 \mu\text{m}$ step size (z direction). Between each 3D image the probe was moved by approximatively 1-2 mm. Metrics extracted from the analysis of LC-OCT images using deep learning algorithms are thickness of skin layers (SC and viable epidermis),

undulation of the dermo epidermal junction (DEJ), the number of cell layers, and cellular metrics (cellular density, shape of the nuclei (volume/compactness) in the epidermal layer and cell network atypia).

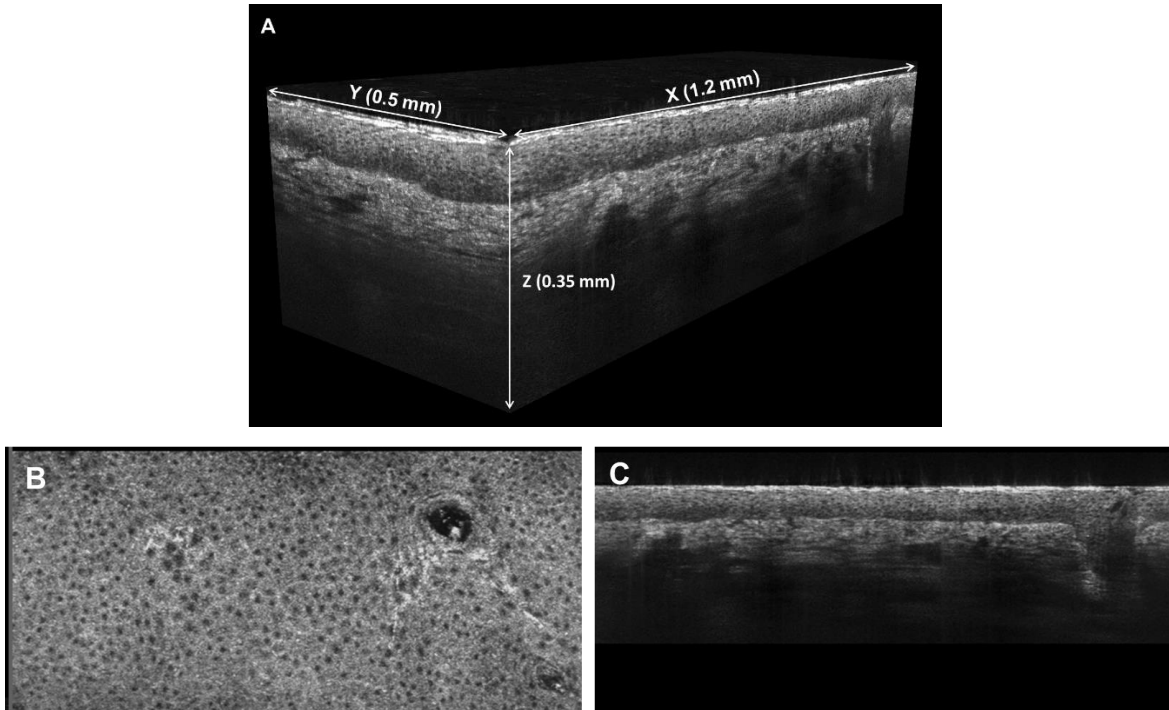


Figure 1: Example of LC-OCT images on healthy skin. A: 3D stack, B: 2D horizontal image (xy) and C: 2D reconstructed vertical image (xz)

LC-OCT® images analysis

Thickness of layers and DEJ segmentation: First, 2D U-net models were applied to segment each reconstructed vertical image (Figure 1B) to allow the prediction of 3 classes of pixels corresponding to the different skin interfaces: i.e. pixels below the skin surface, below the SC and below the dermo-epidermal junction (Figure 2). Second, in order to obtain a 3D result, the algorithm was applied to all vertical views in both xz and yz directions. Third, the outcome of the segmentations for 3D LC-OCT images was checked by a trained operator and regions that correspond to hair follicles were exclude from the calculation of the metrics. The SC thickness and viable epidermis thickness are respectively derived from average numbers of pixels between the segmented skin surface and segmented SC interface; and the segmented SC and the segmented DEJ (Figure 2).

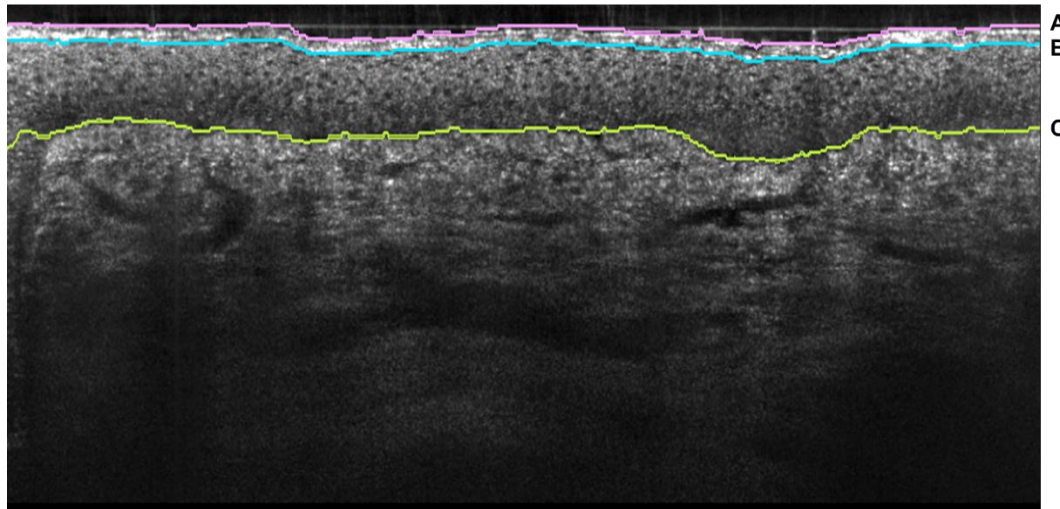


Figure 2 : Segmentation of layers. A: Skin surface, B: SC-Viable epidermis interface and C: Epidermis-Dermis interface (i.e. dermal- epidermal junction)

The DEJ undulation was defined as the surface area of the dermo-epidermis interface normalised by the area of the analysed field of view [17].

The DEJ undulation index was calculated as followed [18]:

$$U_{dej} = (S_{DEJ} / S_{ROI}) - 1,$$

with S_{DEJ} being the area of the DEJ layer and S_{ROI} being the total horizontal area of the LC-OCT image without areas corresponding to hair follicles.

Cellular metrics: For the segmentation of keratinocytes, a deep learning model (AI algorithm) based on 3D convolutions was used as described previously [17]. The architecture used was 3D StarDist model [19] since it detects 3D star-convex shapes at instance level, similar to keratinocyte nuclei. This deep learning model, based on a variant of a 3D ResNet18, was trained from scratch without transfer learning as no known pretrained weights were available for a similar task up to now. StarDist3D uses 3D convolutions to predict at voxel level (3D pixel) the probability of being the centre of a nucleus and the length of the different radii defining the nucleus. 96 radii were used, defined from a 3D Fibonacci lattice, to accurately account for 3D nuclei diversity. The probability threshold for cell detection and the Non-Maximum Suppression threshold were set to 0.5 and 0.05, respectively, allowing touching but non-overlapping cells to be detected. Additional details are provided in the study reported by Chauvel-Picard et al [17].

From the segmentations of all cells of the viable epidermis, the following metrics were calculated: cell density, volume and shape of the cell nuclei, the number of cell layers as well as cell network atypia.

Cell density expressed as cell number/mm² is the total number of nuclei in the epidermis divided by skin surface area.

Nucleus volume was expressed in μm^3 and computed using star-convex polyhedra for the detection and segmentation of cell nuclei. For each 3D stack, the nuclei were sorted by their volume and separated into five categories, from the smallest (quintile I) to the largest (quintile V), each quintile containing 20% of the total number of nuclei ([Figure 3](#)).

Nucleus compactness was used as an indicator of sphericity that was calculated from the 3D surface area of the nucleus (A) and cell volume (V) ($36\pi V^2/A^3$). The compactness is expressed with scores ranging from 0 to 1, where 1 represents a perfect sphere. For each 3D stack, similarly to nucleus volume, quintile I (less compact) to quintile V (most compact) were calculated.

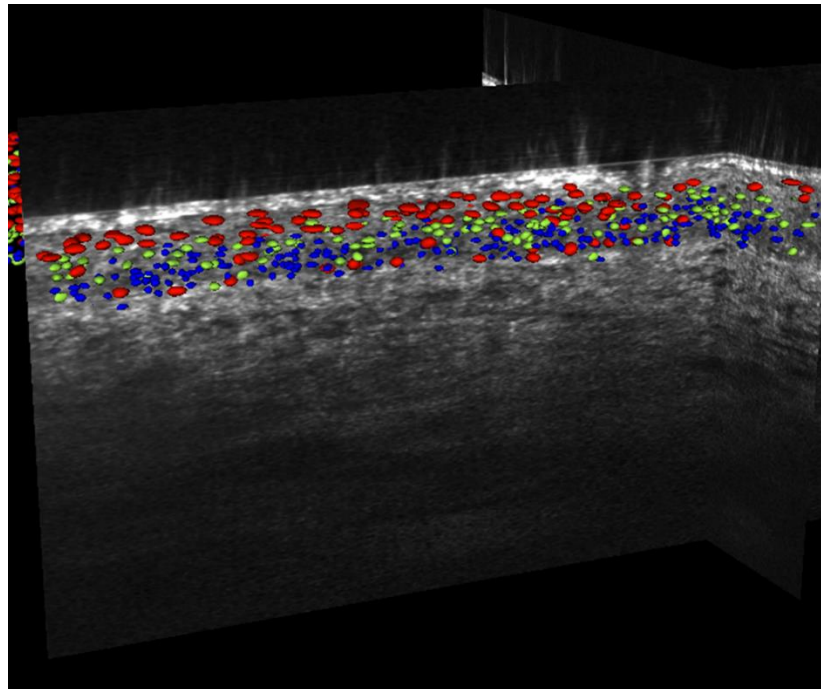


[Figure 3](#): Illustration for cell segmentation. Blue : Smallest cells corresponding to quintile I, Green: intermediate cells corresponding to quintile II, and Red: Largest cells corresponding to quintile V.

The number of cell layers was calculated from the average number of cells crossed on the vertical axis between the SC/SG junction and the DEJ interface.

Cell network atypia can be considered as the detection of outliers in the cell population using features derived from nuclei segmentation. The results are binary scores classifying nucleus as atypical or not. For this purpose, the algorithm was trained using pathological and healthy skins based on the assumption that atypical nuclei occur during pathological process such as actinic keratosis or Squamous cell carcinoma. More details about the model used (XGBoost [20]) can be found in [21]. Presently, the analysis was performed on each 3D stack individually.

Cellular maturation: Cellular metrics can be analysed as function of depth in the viable epidermis. The number of cell layers displayed intra and inter volunteer variability therefore the distribution of metrics was subdivided into 5 depth indexes between 0, corresponding to the deeper part of the epidermis at the interface with the dermis, and 1 that represents the upper part at the interface with the SC. Presently, the nucleus compactness, nucleus volume and cell network atypia were studied.

Statistical analysis: Statistical analysis were performed using MATLAB (MathWorks, USA). Quantitative variables were described by means, standard deviations, minimum, maximum, median, q1, q3. For each quantitative variable allowing to qualify the skin of the subjects, an ANOVA was carried out in order to compare the subjects according to the age groups. The normality of the ANOVA residues was assessed by a Shapiro-Wilk test, with a significance level set at 10%. In the event that the normality of the residuals was not verified, a Kruskal-Wallis test was used as an alternative. When ANOVA (or Kruskal-Wallis test) was significant, a post-hoc test was performed to compare age groups two to two, with Tukey's adjustment to account for multiple comparisons.

Results

1) Thickness of skin layers

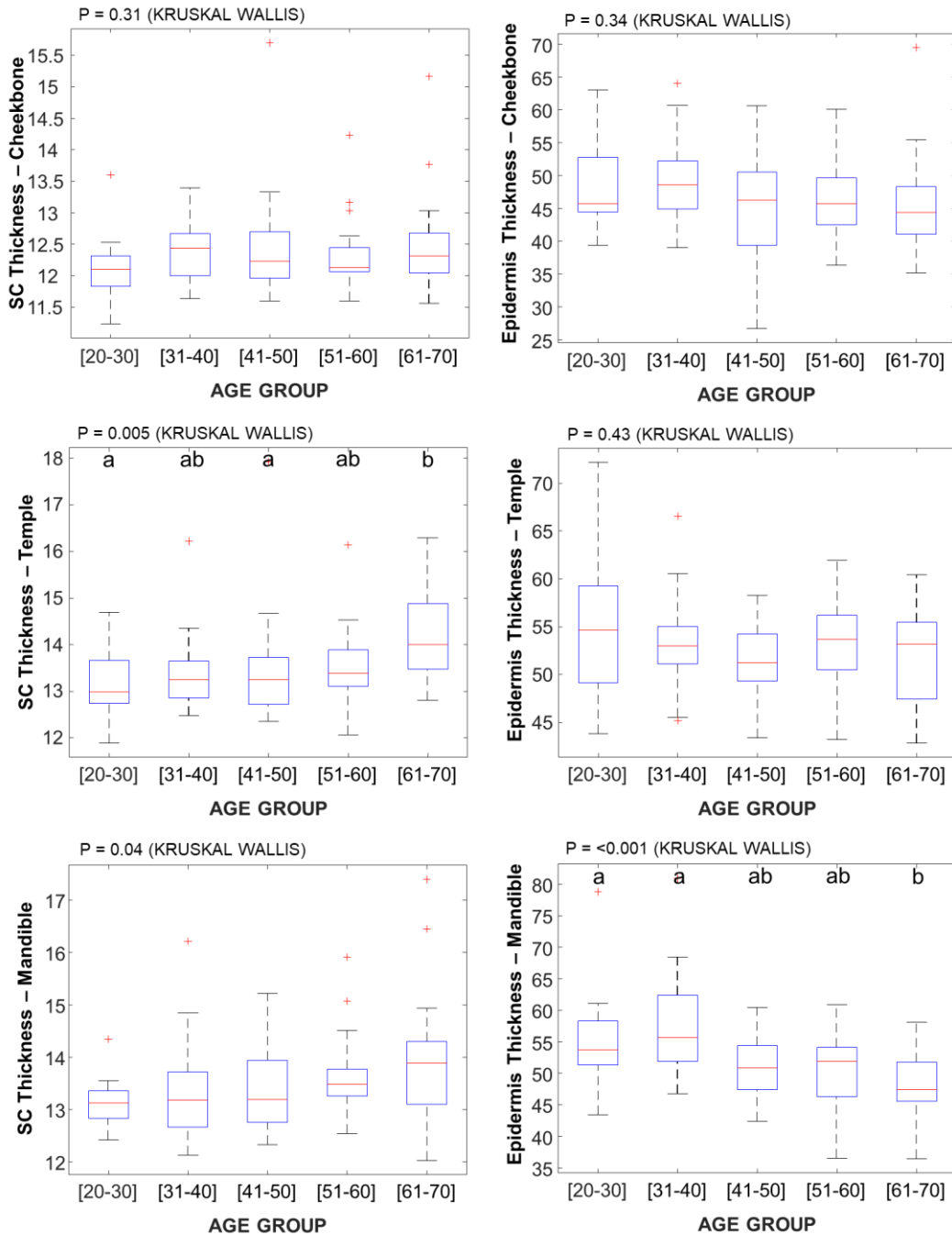


Figure 4: Thickness of skin layers measured with LC-OCT on the cheekbone, temple and mandible according to age groups. Results from pairwise comparisons among age groups are indicated above boxes: two age groups that do not share a common letter are significantly different.

Boxplots in [Figure 4](#) present the SC thickness and viable epidermis thickness determined by LC-OCT on the cheekbone, temple and mandible (inferior jawline) as box plots. The central red line inside the box corresponds to the median value, the top and bottom edges of the blue box are respectively the Q3 (third quartile) and Q1 (first quartile) values and the whiskers indicate the maximum and minimum values. Outliers are represented by red marks.

For the cheekbone, median values for SC thickness display little variations with respectively 12.1 μ m (age group [20,30]), 12.4 μ m (age group [31,40]), 12.2 μ m (age group [41,50]), 12.1 μ m (age group [51,60]) and 12.3 μ m (age group [61,70]) ([Figure 4](#)). The KRUSKAL WALLIS ($p = 0.31$) confirms no significant difference was observed. For the temple, the median value for age group [20,30] was 13.0 μ m compared to 14.0 μ m for the age group [61,70]. The KRUSKAL WALLIS ($p=0.005$) confirms significant differences in SC thickness between age groups while the pairwise comparisons indicates that age group [61,70] is statistically different from age group [20,30] ($p = 0.008$). Similarly, for the mandible the SC thickness displayed an increase from 13.1 μ m (age groups [20,30]) to 13.9 μ m (age group [61,70]) with a p value from KRUSKAL WALLIS = 0.04, and with the main difference observed for the last age group compared to others. The thickness of the viable epidermis determined from LC-OCT images showed limited variations for the cheekbone (KRUSKAL WALLIS $p = 0.34$) and the temple (KRUSKAL WALLIS $p = 0.43$) however a thinning is observed for the mandible (KRUSKAL WALLIS $p < 0.001$) that exhibited median values of 53.7 μ m and 47.5 μ m for respectively age groups [20,30] and [61,70]. The multiple comparison test highlighted that age group [61,70] is different from age groups [20,30] and [31,40] while age groups [41,50] and [51,60] are not separated from either younger or older volunteers.

2) Cellular metrics

For the mandible, cell surface density (ANOVA $p<0.001$), cell compactness (KRUSKAL WALLIS $p=0.043$), cell volume (KRUSKAL WALLIS $p = 0.011$), standard deviation of cell volume (KRUSKAL WALLIS <0.001) and cell network atypia (KRUSKAL WALLIS $p < 0.001$) displayed significant differences between age groups. The mean cell surface density decreases from 31640+/-4247 cells/mm² for age group [20,30] to 26835+/-3511 cells/mm² for age group [61,70] and the multiple comparison test showed that age groups [20,30]/[31,40] were significantly different from age groups [51,60]/[61,70] ([Table 1](#)). Cell compactness exhibits a slight decrease from 0.78+/-0.01 (age group [20,30]) to 0.77+/-0.01 (age group [61,70]) but age groups could not be separated.

Cell volume tends to increase with means equal to $148+/-10 \mu\text{m}^3$ and $158+/-11 \mu\text{m}^3$ for respectively the first and last age groups that are found significantly different, however age groups [31,40], [41,50] and [51,60] do not belong to a different subgroup and are rather an intermediate cluster. While cell volume does not enable to separate age groups, the standard deviation of this metric, that is calculated for each 3D stack individually, displays higher variations with age groups (KRUSKAL WALLIS $p<0.001$) ([Figure 5](#)). The mean values increase from $69+/-5$ (age group [20,30]) to $79+/-10$ (age group [61,70]) and the 2 age groups were found significantly different with the pairwise analysis.

Cell network atypia increases according to age group with respectively $0.170+/-0.03$ (age group [20,30]), $0.18+/-0.03$ (age group [31,40]), $0.20+/-0.04$ (age group [41,50]), $0.21+/-0.04$ (age group [51,60]) and $0.22+/-0.05$ (age group [61,70]). The multiple comparison test further highlights the evolution of this metric according to age with the first and last groups identified as different subgroups while intermediate age groups reflect the gradual increase of cell network atypia values with aging.

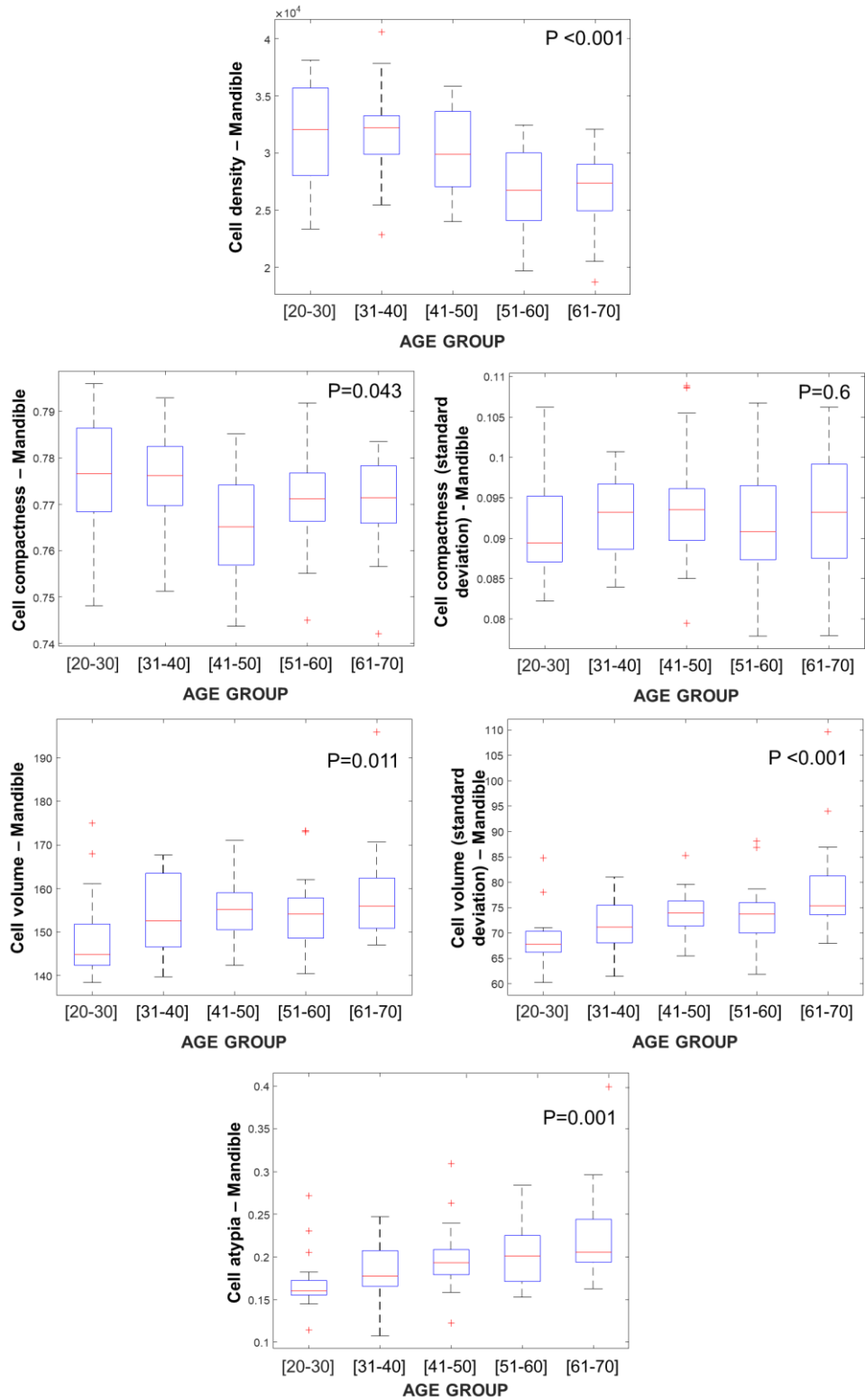


Figure 5: Cellular metrics determined from the LC-OCT for the mandible according to age groups.

Table 1: Summary of cellular metrics for the mandible. Results from pairwise comparisons (multiple comparison test) among age groups are indicated: two age groups that do not share a common letter are significantly different.

Parameters		[20,30]	[31,40]	[41,50]	[51,60]	[61,70]
Cell surface density (cell/mm ²)	Mean (sd)	31641 (4247)	31940 (4117)	30220 (3630)	26888 (3700)	26835 (3511)
	Med [Q1-Q3]	32037 [28186-35705]	32242 [29952-33122]	29895 [27116-33592]	26754 [24083-30015]	27384 [25092-28846]
	Min-Max	23379-38153	22848-40607	24000-35825	19683-32474	18724-32077
Cell compactness	Mult. comp.	a	a	ab	b	b
	Mean (sd)	0.78 (0.01)	0.77 (0.01)	0.77 (0.01)	0.77 (0.01)	0.77 (0.01)
	Med [Q1-Q3]	0.78 [0.77-0.79]	0.78 [0.77-0.78]	0.77 [0.76-0.77]	0.77 [0.77-0.78]	0.77 [0.77-0.78]
Cell compactness (standard deviation)	Min-Max	0.75-0.80	0.75-0.79	0.74-0.79	0.75-0.79	0.74-0.78
	Mult. comp.	-	-	-	-	-
	Mean (sd)	0.09 (0.01)	0.09 (0.01)	0.09 (0.01)	0.09 (0.01)	0.09 (0.01)
Cell volume (μm ³)	Med [Q1-Q3]	0.09 [0.09-0.09]	0.09 [0.09-0.10]	0.09 [0.09-0.10]	0.09 [0.09-0.10]	0.09 [0.09-0.10]
	Min-Max	0.08-0.11	0.08-0.10	0.08-0.11	0.08-0.11	0.08-0.11
	Mult. comp.	-	-	-	-	-
Cell network atypia	Mean (sd)	148 (10)	154 (9)	155 (7)	154 (9)	158 (11)
	Med [Q1-Q3]	144 [143-151]	152 [147-163]	155 [151-158]	154 [149-157]	156 [151-162]
	Min-Max	138-175	140-168	142-171	140-173	147-196
Cell volume (Standard deviation)	Mult. comp.	a	ab	ab	ab	b
	Mean (sd)	69 (5)	71 (6)	74 (4)	74 (6)	79 (10)
	Med [Q1-Q3]	68 [66-70]	71 [68-75]	74 [72-76]	74 [70-76]	75 [74-81]
Cell network atypia	Min-Max	60-85	61-81	65-85	62-88	68-110
	Mult. comp.	a	ab	bc	bc	c
	Mean (sd)	0.17 (0.03)	0.18 (0.03)	0.20 (0.04)	0.21 (0.04)	0.22 (0.05)
Cell network atypia	Med [Q1-Q3]	0.16 [0.17-0.16]	0.17 [0.17-0.21]	0.19 [0.18-0.21]	0.20 [0.17-0.22]	0.21 [0.19-0.24]
	Min-Max	0.11-0.27	0.11-0.25	0.12-0.31	0.15-0.28	0.16-0.40
	Mult. comp.	a	ab	abc	bc	c

For the temple (data not shown), decrease of the cell surface density from 30291+/-3942 cells/mm² (age group [20,30]) to 26049+/-3574 cells/mm² (age group [61,70]) (ANOVA p = 0.019), increase of cell volume from 145+/-6 μm³ (age group [20,30]) to 150+/-9 μm³ (age group [61,70]) (KRUSKALWALLIS p = 0.096) and increase of cell network atypia from 0.21+/-0.02 (age group [20,30]) to 0.25+/-0.03 (age group [61,70]) (ANOVA p <0.001) were also observed.

For the cheekbone (data not shown), the mean cell volume increased from 156+/-8 μm³ (age group [20,30]) to 160+/-12 μm³ (age group [61,70]) (ANOVA p = 0.5) that didn't enable to

differentiate the different age groups, however similarly to the mandible the standard deviation for cell volume displayed greater variability with respectively 72+/-5 and 78+/-8 (ANOVA p = 0.002). The multiple comparison test on the cell volume standard deviation identified the age group [61,70] as significantly different. The cell compactness exhibited a slight decrease from 0.77+/-0.01 age group [20,30] to 0.75+/-0.16 age group [61,70] (ANOVA p < 0.001). However, no significant variation in cell network atypia and cell surface density was found with respective mean values ~0.24 and ~26000 cells/mm² for all age groups.

Interestingly the analysis also enables to compare metrics from different facial skin areas. For instance, taking age group [20,30] as example, the cell surface density appears lower for the cheekbone (26936+/-3849 cells/mm²) compared to mandible (31600+/-4246 cells/mm²) and temple (30291+/-3942 cells/mm²) while the mean cell volume is found higher with 156+/-8 μm³ (cheekbone) compared to 148+/-9.7 μm³ (mandible) and 145+/-6 μm³ (temple). Cell network atypia display significant differences with 0.24+/-0.02 for the cheekbone compared to 0.17+/-0.03 for the mandible and 0.21+/-0.02 for the temple.

3) Metrics as function of depth (cell maturation)

When performing 3D imaging with techniques like LC-OCT, the information (i.e. cellular metrics) can be interpreted as function of depth within the tissue (*see material and methods*). [Figure 6 A](#) and [6 B](#) present nucleus compactness and cell network atypia in the viable epidermis for the mandible. It was observed that for all age groups the evolution of cell compactness follows the same pattern with mean values decreasing from ~0.8 for the depth index 0 (interface dermis / epidermis) to ~0.65 for the depth index 1 (interface living epidermis / SC) ([Figure 6A](#)). These variations somehow reflect the cell maturation from basal layer to stratum granulosum, and they provide insight into modifications of cellular shapes and size during the process. For instance, for nucleus compactness, at depth index 0.5 and 0.75, a difference is seen between the age groups. [Figure 6C](#) shows the boxplots constructed from metrics at the depth index 0.5. A decrease as function of age groups was found. Cell network atypia also displays a decrease as function of depth indexes ([figure 6B](#)). Although the means are comparable at depth index 0 (~0.23-0.24), at depth index 1 the means values significantly differ. The boxplots for the depth index 0.5 in [figure 6B](#) confirm the increase in

cell network atypia as function of age groups. [Table 2](#) gathers mean values for nucleus compactness and cell network atypia for the mandible. For nucleus compactness it is observed that there are no significant differences between age groups for depth indexes 0 ($p = 0.279$) and 0.25 ($p=0.236$), however for depth indexes 0.5, 0.75 and 1 the ANOVA delivered respectively $p = 0.035$, $p= 0.001$ and $p= 0.001$. For the cell network atypia, at depth index 0 there is also no significant differences between age groups, but like nucleus compactness it is in skin layers closer to the SC that values differ. At depth index 0.5 ($p=0.001$), the mean value for age group [20,30] is significantly lower ($0.169+/-0.044$) compared to age group [61,70] ($0.241+/-0.073$). This difference is still observed at depth index 1 ($p<0.001$) with mean values equal to $0.106+/-0.017$ (age group [20,30]) and $0.162+/-0.074$ (age group [61,70]). For nucleus volume, only depth index 0.75 ($p=0.017$) and depth index 1 ($p=0.002$) shows significant differences with respectively means values increasing from $165.3+/-17.5 \mu\text{m}^3$ to $188.5+/-28.3 \mu\text{m}^3$ and $220.1+/-6.7 \mu\text{m}^3$ to $245.1+/-25 \mu\text{m}^3$ for age groups [20,30] and [61,70] ([Table 2](#)).

Similar observations were made for the temple and cheekbone (data not shown). For example, the cell network atypia for the temple at depth index 0.5 exhibit values equal to $0.153+/-0.028$ for age group [20,30] and $0.199+/-0.048$ for age group [60,70]. At depth index 1, a similar difference is observed between the 2 age groups with atypia $0.115+/-0.017$ and $0.152+/-0.044$. Similarly for the cheekbone, cell network atypia at depth index 1 is $0.115+/-0.017$ and $0.143+/-0.034$ for age groups [20,30] and [61,70] while cell volume at the same depth index was found to be $222.65+/-17.2 \mu\text{m}^3$ and $236.07+/-29.7 \mu\text{m}^3$ for the same age groups.

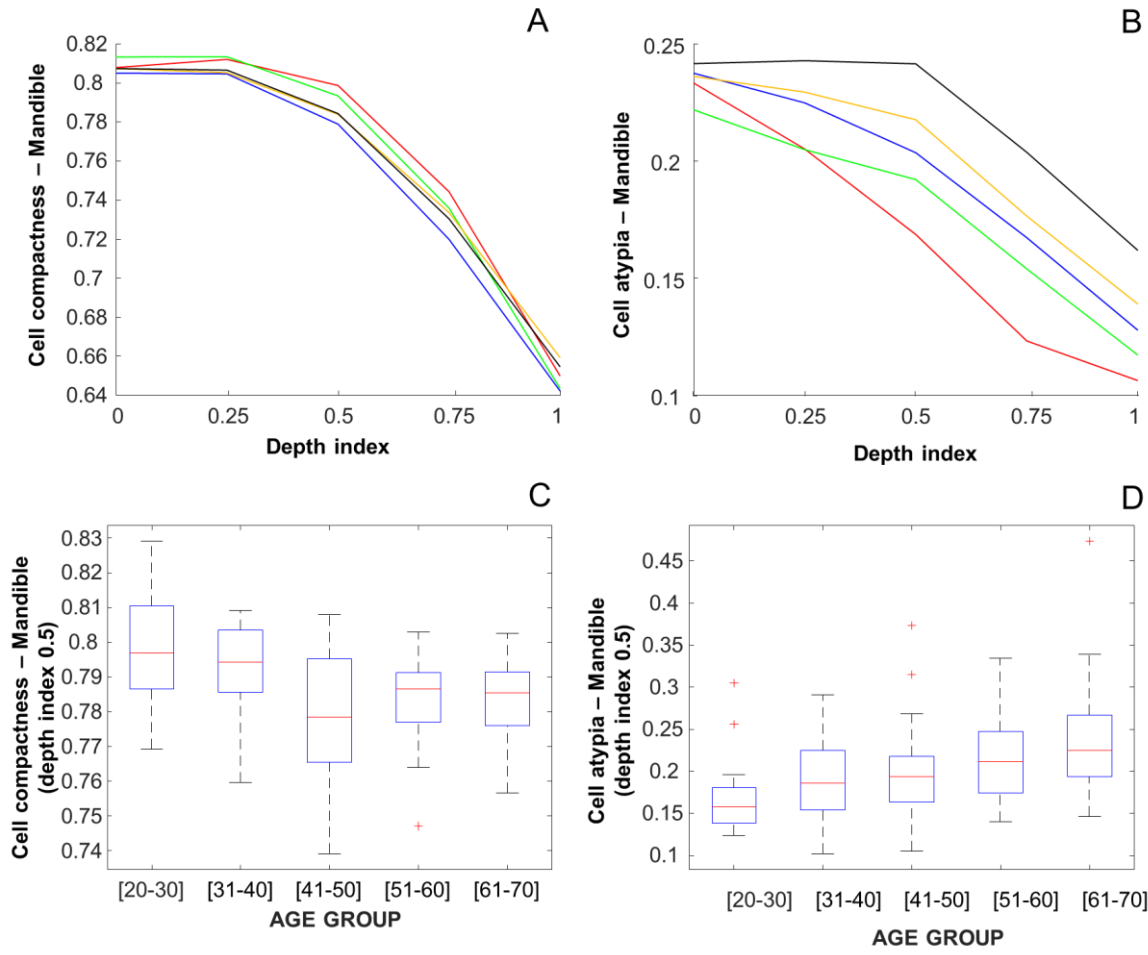


Figure 6 Examples of metrics studied as function of depth for the mandible, for each age group. Relative index is given as depth index scores from 0 (interface viable epidermis/dermis) to 1 (interface epidermis/SC). A: Means for cell compactness, B: Means for cell atypia, C: Box plot at relative depth 0.5 for cell compactness and D: Box plot at relative depth 0.5 for cell atypia. Red: age group [20,30], green: age group [31,40], blue: age group [41,50], yellow: age group [51,60] and black: age group [61,70]

Table 2 Summary of cellular metrics as function of depth index (Mandible)

Parameters		Depth index 0	Depth index 0.25	Depth index 0.5	Depth index 0.75	Depth index 1
Nucleus compactness Mean (sd)	[20,30]	0.808 (0.018)	0.812 (0.016)	0.799 (0.016)	0.744 (0.017)	0.650 (0.027)
	[31,40]	0.813 (0.013)	0.813 (0.010)	0.793 (0.012)	0.736 (0.016)	0.644 (0.026)
	[41,50]	0.805 (0.009)	0.805 (0.010)	0.779 (0.019)	0.720 (0.028)	0.642 (0.023)
	[51,60]	0.807 (0.012)	0.805 (0.010)	0.784 (0.013)	0.734 (0.022)	0.659 (0.026)
	[61,70]	0.807 (0.008)	0.806 (0.008)	0.784 (0.011)	0.730 (0.020)	0.654 (0.026)
	P value	0.279	0.236	0.035	0.001	0.001

Parameters		Depth index 0	Depth index 0.25	Depth index 0.5	Depth index 0.75	Depth index 1
Cell network Atypia Mean (sd)	[20,30]	0.233 (0.036)	0.205 (0.044)	0.169 (0.044)	0.123 (0.028)	0.106 (0.017)
	[31,40]	0.222 (0.025)	0.205 (0.037)	0.192 (0.048)	0.154 (0.043)	0.117 (0.023)
	[41,50]	0.237 (0.023)	0.225 (0.042)	0.203 (0.062)	0.167 (0.055)	0.128 (0.024)
	[51,60]	0.236 (0.027)	0.229 (0.045)	0.218 (0.057)	0.176 (0.056)	0.139 (0.030)
	[61,70]	0.241 (0.018)	0.243 (0.043)	0.241 (0.073)	0.204 (0.086)	0.162 (0.074)
	P value	0.193	0.022	0.002	0.001	<0.001
Nucleus volume (μm^3) Mean (sd)	[20,30]	127.8 (7.0)	128.6 (7.6)	138.5 (11.9)	165.3 (17.5)	220.1 (6.7)
	[31,40]	125.8 (4.4)	129.7(6.0)	145.0 (13.0)	180.9 (19.1)	235.1 (23.0)
	[41,50]	129.8 (3.6)	131.5 (5.6)	144.8 (9.6)	182.6 (15.6)	237.1 (16.0)
	[51,60]	130.4 (7.4)	131.8 (5.1)	145.5 (10.9)	180.0 (24.3)	224.8 (21.9)
	[61,70]	131.8 (5.6)	133.0 (5.8)	147.9 (15.0)	188.5 (28.3)	245.1 (25.0)
	P value	0.016	0.163	0.175	0.017	0.002

Discussion.

LC-OCT imaging couple to AI is a powerful approach enabling *in vivo* 3D visualisation of skin structures. The micrometric resolution of the system allowed to derive histological and cellular metrics from the 3D stacks to deliver quantitative analysis of healthy facial skin ageing. A previous study by Monnier *et al.* conducted on seven body sites from 29 young volunteers (mean age = 25.9 years) using 2D LC-OCT imaging [22] showed significant variations in the thickness of skin layers and DEJ undulation, especially between hand and cheek. These observations were confirmed by Chauvel-Picard *et al.* with an investigation including 8 female volunteers with age ranging from 20 to 60 years old [17]. Additionally, it was highlighted that cell density (cell/mm²), Number of cell layers, nucleus volume and nucleus compactness are quantitative cellular metrics exhibiting significant differences according to body sites. The present study however emphasised on the investigation of age-related variation in facial skin from a much larger cohort of volunteers (n=100), targeting 3 zones, i.e. cheekbone, temple and mandible. Using the same age group [20,30] for comparison, the thickness of the SC found, i.e. cheekbone = 12.1+/-0.5 μm , temple = 13.2+/-0.8 μm and mandible = 13.1+/-0.4 μm , are higher compared to the 2 previous studies that respectively reported means equal 9+/-1 μm and 9.7+/-1.6 μm [17,22]. That is potentially explained by the different area analysed (cheekbone versus cheek). The epidermis thickness is however consistent with respectively 48.4+/-6.5 μm (cheekbone), 54.5+/-6.5 μm

(temple) and $55.1+/-7.2\text{ }\mu\text{m}$ (mandible) in the present study compared to $59.4+/-4.6\text{ }\mu\text{m}$ and $58.7+/-8.7$. Moreover, it was also confirmed the flatness of the DEJ and the number of cell layers (~5) for the cheek area (data not shown) hence they do not represent relevant metrics for the study of age-related modifications. The cell density displayed substantial differences with $42\ 823+/-3021\text{ cells/mm}^2$ reported for the cheek by Chauvel-Picard *et al.* while presently means calculated were lower with $26936+/-3849\text{ cells/mm}^2$ (Cheekbone), $30291+/-3942\text{ cells/mm}^2$ (Temple) and $31641+/-4247\text{ cells/mm}^2$ for the mandible. However, the means calculated in this study for the age group [20,30] alone resulted from 180 3D stacks. It was found that cell density decreases with age that can be a result of the decreased mitotic activity and increased duration of cell cycle observed with ageing [23]. Nevertheless, the most relevant observation is the distribution cellular metrics according to depth in the viable epidermis. This layer consists primarily of keratinocytes (~95% of cells), Langerhans cells (~2%), melanocytes (~3%) and Merkel cells (~0.5%) [24], therefore it can be considered that results reflected the maturation of keratinocytes. The cell nucleus compactness and volume indicate that smaller and more spherical cells are located deeper in the epidermis, at a depth index corresponding to the basal layer ([Figure 6](#)). The decreasing in compactness and the increase in volume for depth indexes closer to the SC (outer part of the epidermis) highlight the sensitivity of LC-OCT to detect and monitor modifications in cell shape and size correlated with cell maturation [25]. The literature about visualization of impairment of cell morphology is mainly limited to characterization from 2D histological or microscopic horizontal sections [10,26,27]. LC-OCT enabled quite uniquely to quantify the variations in cellular metrics according to age but also to interpret results according to distribution across 3D stacks. Results demonstrated the feasibility to determine keratinocyte abnormalities with aging that can result from the loss of polarity and a disorderly maturation [28,29], that can be used as biomarkers. This is the first exploratory investigation focusing on facial skin ageing in healthy volunteers and aiming at acquiring biological knowledge about the chronological and photoaging processes. Advanced *in vivo* imaging such as LC-OCT coupled to AI have a key role to play for the understanding microstructural and (sub-)cellular mechanisms involved.

Conclusion.

3D LC-OCT imaging coupled to AI algorithms enabled to quantify several histological and cellular epidermal parameters (metrics). The technique is a powerful approach to study age-related modifications hence it provides a unique tool to better comprehend the process at a micrometric level. Moreover, the method could have valuable inputs for investigating efficacy of cosmetic topical products. Presently, accessing detailed information about cells maturation and correlating variations with age groups open perspectives for further exploratory studies. Nuclei volume, compactness and atypia of the cell network have been identified as potential key biomarkers to quantify skin ageing in healthy female volunteers.

Conflict of Interest Statement. Mélanie Pedrazzani, Sébastien Fischman and Théo Viel are DAMAE Medical employees. All other authors had no conflict of interest to declare.

References.

1. Hofmeier SM, Runfola CD, Sala M, et al. (2016) Body image, aging, and identity in women over 50: The Gender and Body Image (GABI) study. *J Women Aging* 29: 1-12.
2. Flament F, Amar D, Feltin C, et al. (2018) Evaluating age-related changes of some facial signs among men of four different ethnic groups. *Int J Cosmetic Sci* 40: 502-515.
3. Luebberding S, Krueger N, Kerscher M (2014) Mechanical properties of human skin in vivo: a comparative evaluation in 300 men and women. *Skin Res Technol* 20: 127-135.
4. Vergilio MM, Vasques LI, Leonardi GR (2021) Characterization of skin aging through high-frequency ultrasound imaging as a technique for evaluating the effectiveness of anti-aging products and procedures: A review. *Skin Res Technol* 27: 966-973.
5. Longo C, Casari A, Beretti F, et al. (2013) Skin aging: In vivo microscopic assessment of epidermal and dermal changes by means of confocal microscopy. *J Am Acad Dermatol* 68: e73-e82.
6. Ulrich M, Lange-Asschenfeldt S (2013) In vivo confocal microscopy in dermatology: from research to clinical application. *J Biomed Opt* 18: 061212-061212.
7. Ilie MA, Caruntu C, Lupu M, et al. (2019) Current and future applications of confocal laser scanning microscopy imaging in skin oncology. *Oncol Lett* 17: 4102-4111.

8. Ilie MA, Caruntu C, Lixandru D, et al. (2019) In vivo confocal laser scanning microscopy imaging of skin inflammation: Clinical applications and research directions. *Exp Ther Med* 17: 1004-1011.
9. Sugata K, Osanai O, Sano T, et al. (2011) Evaluation of photoaging in facial skin by multiphoton laser scanning microscopy. *Skin Res Technol* 17: 1-3.
10. Rajadhyaksha M, González S, Zavislan JM, et al. (1999) In vivo confocal scanning laser microscopy of human skin II: advances in instrumentation and comparison with histology. *J Investigative Dermatology* 113: 293-303.
11. Welzel J, Lankenau E, Birngruber R, et al. (1997) Optical coherence tomography of the human skin. *J Am Acad Dermatol* 37: 958-963.
12. Gambichler T, Boms S, Stücker M, et al. (2006) Epidermal thickness assessed by optical coherence tomography and routine histology: preliminary results of method comparison. *J Eur Acad Dermatol* 20: 791-795.
13. Boone M, Jemec GBE, Marmol VD (2012) High-definition optical coherence tomography enables visualization of individual cells in healthy skin: comparison to reflectance confocal microscopy. *Exp Dermatol* 21: 740-744.
14. Dubois A, Levecq O, Azimani H, et al. (2018) Line-field confocal optical coherence tomography for high-resolution noninvasive imaging of skin tumors. *J Biomed Opt* 23: 106007-106007.
15. Ogien J, Levecq O, Azimani H, et al. (2019) Dual-mode line-field confocal optical coherence tomography for ultrahigh-resolution vertical and horizontal section imaging of human skin in vivo. *Biomed Opt Express* 11: 1327-1335.
16. Pedrazzani M, Breugnot J, Rouaud-Tinguely P, et al. (2020) Comparison of line-field confocal optical coherence tomography images with histological sections: Validation of a new method for in vivo and non-invasive quantification of superficial dermis thickness. *Skin Res Technol* 26: 398-404.
17. Chauvel-Picard J, Bérot V, Tognetti L, et al. (2022) Line-field confocal optical coherence tomography as a tool for three-dimensional in vivo quantification of healthy epidermis: A pilot study. *J Biophotonics* 15: e202100236.
18. Timár F, Soós G, Szende B, et al. (2000) Interdigitation index - a parameter for differentiating between young and older skin specimens: Interdigitation index. *Skin Res Technol* 6: 17-20.
19. Weigert M, Schmidt U, Haase R, et al. (2020) Star-convex Polyhedra for 3D Object Detection and Segmentation in Microscopy. *2020 Ieee Winter Conf Appl Comput Vis Wacv* 00: 3655-3662.
20. Krishnapuram B, Shah M, Smola A, et al. (2016) XGBoost. *Proc 22nd Acm Sigkdd Int Conf Knowl Discov Data Min* 785-794.
21. Fischman S, Pérez-Anker J, Tognetti L, et al. (2022) Non-invasive scoring of cellular atypia in keratinocyte cancers in 3D LC-OCT images using Deep Learning. *Sci Rep-uk* 12: 481.

22. Monnier J, Tognetti L, Miyamoto M, et al. (2020) In vivo characterization of healthy human skin with a novel, non-invasive imaging technique: line-field confocal optical coherence tomography. *J Eur Acad Dermatol* 34: 2914-2921.
23. Zouboulis CC, Makrantonaki E (2011) Clinical aspects and molecular diagnostics of skin aging. *Clin Dermatol* 29: 3-14.
24. Tobin DJ (2017) Introduction to skin aging. *J Tissue Viability* 26: 37-46.
25. Koster MI (2009) Making an Epidermis. *Ann Ny Acad Sci* 1170: 7-10.
26. Huzaira M, Rius F, Rajadhyaksha M, et al. (2001) Topographic Variations in Normal Skin, as Viewed by In Vivo Reflectance Confocal Microscopy. *J Invest Dermatol* 116: 846-852.
27. Koehler MJ, Zimmermann S, Springer S, et al. (2011) Keratinocyte morphology of human skin evaluated by in vivo multiphoton laser tomography. *Skin Res Technol* 17: 479-486.
28. GILCHREST BA, YAAR M (1992) Ageing and photoageing of the skin: observations at the cellular and molecular level. *Brit J Dermatol* 127: 25-30.
29. MAKRANTONAKI E, ZOUBOULIS CC (2007) Molecular Mechanisms of Skin Aging. *Ann Ny Acad Sci* 1119: 40-50.